# Monte Carlo Simulations of Polyion−Macroion Complexes. 2. Polyion Length and Charge Density Dependence†

**Anna Akinchina* and Per Linse**

*Physical Chemistry 1, Center for Chemistry and Chemical Engineering, Lund University, Box 124, SE-221 00 Lund, Sweden*

*Received: November 20, 2002*

The complexation between a polyion and an oppositely charged spherical macroion in the framework of the primitive model has been studied by the use of Monte Carlo simulations. The polyion length, linear charge density, and bare persistence length are varied systematically, while the properties of the macroion are kept constant. The polyion charge to macroion charge ratio is varied between 1/4 and 4. The structure of the complex is investigated by direct visualization; polyion bead complexation probability; loop, tail, and train characteristics; degree of overcharging; and tail joint probability functions. The strongest complexes are observed for flexible chains, where the polyion is folded around the macroion. In the case of fully flexible chains, a transition from a collapsed state to a fluctuating two-tail state and eventually to a one-tail state are observed as the chain length is increased. As the stiffness is increased, several complex structures, such as multiloop, single-loop, and solenoid arrangements, and finally a structure involving only a single contact between the polyion and the macroion occur. In particular, for long and highly charged polyions, a transition from the one-tail state to a two-tail state appears as the chain stiffness is increased. A discussion with recent theories and other simulation studies is also provided.

## 1. Introduction

The understanding of the complexation between charged polymers and oppositely charged colloids is of immense importance in a large range of biological and technological systems. Such systems contain polyelectrolytes such as DNA, polysaccharides, and polyamines, etc., interacting with compact colloids such as proteins, surfactant micelles and vesicles, dendrimers, and latex particles. Some of the experimental studies in this are summarized by Goddard,[1] Kwak,[2] Lindman and Thalberg,[3] Hansson and Lindman,[4] and Doublier et al.[5] Significant advances on the basis of experimental studies,[6−13] theoretical developments,[14−26] and computer simulations[27−37] have recently been made.

A central aspect in the analytic studies by von Goeler and Muthukumar,[14] Gurovitch and Sens,[15] Park et al.,[16] and Mateescu et al.[17] has been the possibility to overcharge a spherical macroion by an oppositely charged polyelectrolyte. Recently, Netz and co-workers,[18−20] Nguyen and Shklovskii,[21] and Schiessel et al.[22−24] have used more detailed molecular models to examine the 1:1 complexation and to examine the structure of the complex. The complexation in systems containing more than two macroions has been addressed by Nguyen and Shklovskii[25,26] and Schiessel et al.[23]

Regarding simulation studies, Wallin and Linse[27−30] performed a series of Monte Carlo simulations including determination of the free energy of the complexation. Kong and Muthukumar[31] have examined the adsorption of a polyion onto charged curved surfaces also by Monte Carlos simulations. Simulations complementing their theoretical predictions have also been made by Mateescu et al.[17] and by Nguyen and Shklovskii.[21] Extensive investigation has been made by Chodanowski and Stoll who investigated the polyion−macroion complexation at different polyion lengths[32] and sphere sizes[33] and at several screening lengths. Several simulation studies considering complexation of one polyelectrolyte with several macroions,[25,34,35] and solutions containing polyelectrolytes and macroions[36] have been recently presented.

In our previous work, which we will refer to as paper 1,[37] we presented results from Monte Carlo simulations involving one polyion complexing to one macroion of the same absolute charge. The structure and the energetics of the complex were investigated for systematic changes of the chain stiffness at different macroion radii and chain linear charge densities. A very rich structural behavior was obtained, and close similarities with, in particular, a theory developed by Schiessel were obtained.[24]

In the present work, we extend our previous investigation of the complexation between one polyion and one macroion to involve situations where the two species can have different absolute charges. Here, we make systematic changes of the property of the polyion in salt-free systems. In particular, we vary the polyion length, the polyion linear charge density, and the chain flexibility in a wide range, keeping the macroion charge and size constant for all of the systems. Our results qualitatively agree with recent theories,[17,21,24] complement previous simulation results,[32] and provide a comprehensive picture of the structure of the complex for the parameter space studied.

The paper is organized as follows. The model system and some simulation aspects are given in section 2. Section 3 deals with our results, and systems with different chain flexibility will be described separately. Section 4 contains a discussion of recent theoretical and simulation results and some of our results. The paper ends with a summary given in section 5.

† Part of the special issue "International Symposium on Polyelectrolytes".

* To whom correspondence should be addressed. E-mail: Anna.Akinchina@fkem1.lu.se.

10.1021/jp022460f CCC: $25.00 
Published on Web 06/25/2003

## 2. Method

**2.1. Model.** The same model as in paper 1[37] has been used. Briefly, a solution of one polyion, one macroion, and a minimum amount of small ions are enclosed in a sphere using the so-called cell model. The solution is described using the primitive model, implying that the charged species (polyion beads, macroion, and small ions) are represented as charged hard spheres, whereas the solvent (water) is represented by a dielectric continuum characterized only by a relative permittivity. In the present study, the macroion is also fixed at the center of the cell.

The polyion is described as a sequence of $N_b$ charged beads connected by harmonic springs. Each bead has the hard-sphere radius $R_b = 2$ Å and the charge $Z_b$. The total charge of the polyion is hence given by $Z_p = N_b Z_b$. The chain flexibility is controlled by an angular energy term. The macroion has the hard-sphere radius $R_m = 20$ Å and the charge $Z_m = -40$, whereas the small ions have a hard-sphere radius $R_\pm = 2$ Å and a charge $Z_\pm = \pm 1$.

The total potential energy of a system $U$ can be expressed as

$$U = U_{hc} + U_{el} + U_{bond} + U_{angle} + U_{cell} \tag{1}$$

where the terms describing the hard-core repulsion $U_{hc}$ and the Coulomb interaction $U_{el}$ are given by

$$U_{hc} + U_{el} = \sum_{i<j} U_{ij} \tag{2}$$

$$U_{ij} = \begin{cases} \infty & r_{ij} < R_i + R_j \\ \dfrac{Z_i Z_j e^2}{4\pi\epsilon_0\epsilon_r r_{ij}} & r_{ij} \geq R_i + R_j \end{cases} \tag{3}$$

with $R_i$ and $Z_i$ denoting the radius and the charge, respectively, of particle $i$ (the polyion bead, a macroion, or a small ion), $e$ the elementary charge, $\epsilon_0$ the permittivity of vacuum, $\epsilon_r$ the relative permittivity of water, and $r_{ij}$ the distance between the centers of particles $i$ and $j$.

In addition to hard-core and electrostatic interactions, the description of the polyion includes harmonic potentials for bonds and angles. The bond potential energy $U_{bond}$ is given by

$$U_{bond} = \sum_{i=1}^{N_b-1} \frac{k_{bond}}{2}(r_{i,i+1} - r_0)^2 \tag{4}$$

where $r_{i,i+1}$ denotes the distance between two connected segments with the equilibrium separation $r_0 = 5$ Å and the force constant $k_{bond} = 0.4$ N/m. With the other interactions included, the typical root-mean-square (rms) bead−bead separation becomes $\langle R^2_{bb}\rangle^{1/2} \approx 5.5$ Å. The angular potential energy is represented by

$$U_{angle} = \sum_{i=2}^{N_b-1} \frac{k_{angle}}{2}(\alpha_i - \alpha_0)^2 \tag{5}$$

where $\alpha_i$ is the angle formed by the vectors $\mathbf{r}_{i+1} - \mathbf{r}_i$ and $\mathbf{r}_{i-1} - \mathbf{r}_i$ made by three consecutive segments with the equilibrium angle $\alpha_0 = 180°$ and the force constant $k_{angle}$. In addition to the angular potential, the electrostatic interaction among the segments also contributes to the rigidity of the polyelectrolyte, and this electrostatic contribution is of course affected by other ionic particles present.

**TABLE 1: Specification of the Systems Investigated**

| | |
|---|---|
| **General Parameters** | |
| cell radius | $R_{cell} = 1241$ Å |
| temperature | $T = 298$ K |
| relative permittivity | $\epsilon_r = 78.5$ |
| **Polyion** | |
| bead radius | $R_b = 2.0$ Å |
| number of beads | $N_b = 40$, 80, 120, and 160 |
| bead charge | $Z_b = 0.25$, 0.5, 0.75, and 1 |
| bare persistent length | $l_P = 7$, 250, and 1000 Å |
| **Macroion** | |
| radius | $R_m = 20$ Å |
| charge | $Z_m = -40$ |
| **Small Ions** | |
| ion radii | $R_\pm = 2.0$ Å |
| ion charges | $Z_\pm = \pm 1$ |

Finally, the confinement potential energy $U_{cell}$ in eq 1 is given by

$$U_{cell} = \sum_i U_i \tag{6}$$

$$U_i = \begin{cases} 0 & r_i \leq R_{cell} \\ \infty & r_i > R_{cell} \end{cases} \tag{7}$$

where $R_{cell}$ is the radius of the cell. Formally, the confinement potential acts on all particles, but in practice only the small ions are affected. The position of the macroion is fixed at the origin ($\mathbf{r}_m = 0$), and the polyion always forms a complex with the macroion with the polyion contour length $L = \langle R^2_{bb}\rangle^{1/2}(N_b - 1)$ being smaller than $R_{cell}$.

**2.2. Systems.** In the present study, the properties of the polyion are varied, whereas the properties of the macroion are fixed. We consider a variation of (i) polyion length ($N_b$ = 40, 80, 120, and 160), (ii) bead charge ($Z_b$ = 0.25, 0.5, 0.75, and 1), and (iii) polyion flexibility ($l_P$ = 7, 250, and 1000 Å), independently. Hence in total $4 \times 4 \times 3$ different systems are considered. The variation of the bead charge will often be referred to as a variation in the chain linear charge density. The different bare flexibilities were achieved by using $k_{angle}$ = 0, 33.5, and 135 J/(mol deg$^2$), respectively. The bare persistence length $l_P$ was calculated according to $l_P = \langle R^2_{bb}\rangle^{1/2}/(1 + \langle\cos\alpha_i\rangle)$,[37] using a single uncharged polymer. The specifications of the systems are collected in Table 1.

In paper 1, the polyion charge to macroion charge ratio $|Z_p/Z_m|$ was unity throughout. In the present work, the polyion charge ranges from $Z_p = 10$ to $Z_p = 160$, and with $Z_m = -40$ the charge ratio becomes $|Z_p/Z_m| = 1/4$ to 4. The systematic variation of $N_b$ and $Z_b$ enables a detailed examination of how the complexation depends on (i) the polyion charge at constant polyion length (fixed $N_b$ and variable $Z_b$) and (ii) the polyion length at constant linear charge density (variable $N_b$ and fixed $Z_b$). The combination ($N_b$, $Z_b$) = (80, 0.5) corresponds to system I and (40, 1) to system III of paper 1. In those cases where polyion and macroion have different absolute charges, the necessary amount of monovalent small ions was added to keep the total system neutral. Hence, if any, only cations *or* anions were added.

**2.3. Simulation Details.** Structural properties of the model systems were obtained by performing Monte Carlo (MC) simulations in the canonical ensemble, employing the standard Metropolis algorithm.[38] Since the position of the macroion was fixed, only the polyion beads and the small ions were subjected to trial moves. Four different types of MC trial moves were employed: (i) single particle displacement of polyion beads and

small ions, (ii) pivot rotation of parts of the polyion, (iii) translation of the entire polyion, and (iv) slithering move of the polyion. For the polyion, the single particle move was attempted 50 times more often than the other three types of moves. The values of the displacement parameters of the different types of trial moves were selected for each system. The values for trial move of types i−iii were $\Delta_{bead} = 0.7-2.5$ Å, $\Delta_{\alpha} = 15-360°$, and $\Delta_{chain} = 0.3-0.8$ Å, respectively. For the polyion, the acceptance ratios of the four types of trial moves were ≈0.5, ≈0.5, ≈0.7, and ≈0.7, respectively.

As evident from the results below, the strong electrostatic attraction between the polyion and macroions gives rise to a firm complex. To ensure that equilibrium structures are achieved, simulations with two very different initial configurations have been employed. All systems have been simulated using initially separated macromolecules obtained from randomly generated polyion positions and configurations. Simulations were also performed by starting with premade complexes taken from final configurations of simulations of other systems, where the polyion had shorter and/or larger persistence length. Each simulation included typically an equilibration of $5 \times 10^5$ MC passes (trial moves per particle) followed by a production run of $10^6-10^7$ MC passes. Statistical uncertainties were evaluated by dividing the total simulation into typically 10 subbatches and are generally negligible. All the simulations were carried out with the use of the integrated Monte Carlo/molecular dynamics/Brownian dynamics simulation package MOLSIM.[39]

**2.4. Characterization of Polyion−Macroion Complexes.** In the case of a small polyion charge, all, or nearly all, beads are collapsed on the macroion surface. With a large polyion charge, only a part of the polyion is involved and one or two tails are present. We distinguish between a preference for the macroion to complex (i) to the central part of the polyion (symmetric binding) and (ii) toward one side of the polyion (an asymmetric binding). In (i), obviously two tails are present. Furthermore, in (ii) a distinction between a preference for the macroion to complex to (ii.a) a region between the end and the center of the polyion (giving rise to two tails) and (ii.b) the end of the polyion (one tail) can be made.

The complexes have systematically been analyzed by examining (i) snapshots, (ii) bead complexation probability functions, (iii) loop, tail, and train characteristics, and (iv) the degree of overcharging. The nature of the polyion−macroion complexes differs strongly among the systems considered. Therefore, a direct visualization of even a single snapshot provides a good initial description of a complex.

The bead complexation probability function, $P_c(i_b)$, denotes the probability that the bead, $i_b$, is located near (being complexed to) the macroion. Here, we consider a bead to be complexed when the separation between the centers of a bead and the macroion does not exceed the distance $r = R_c \equiv R_m + R_b + 5$ Å. The lower boundary $P_c(i_b) = 0$ implies that bead $i_b$ never is complexed with the macroion, and the upper one $P_c(i_b) = 1$ corresponds to the case in which this bead is always complexed. There is some ambiguity in selecting $R_c$, but the qualitative conclusions are not affected by the precise choice.[37] Since the chain possesses a mirror symmetry, $P_c(i_b)$ should be symmetric with respect to a reflection at $i_b = (N_b + 1)/2$; i.e., $P_c(i_b) = P_c(N_b + 1 - i_b)$. When an *asymmetric binding* appears, the system has to pass a free energy barrier between the two asymmetric states before a *symmetric* complexation probability function is achieved. This occurs in most cases where an asymmetric binding appears. But in a few cases the barrier is too large to allow a symmetric function to be established (with the selected types of trial moves and simulation length), and here both the simulated asymmetric and the symmetrized complexation probability are provided.

The conformation of the complexed polyion has been characterized by quantifying (i) the average number of beads in a loop, tail, and train, (ii) the average number of loops, tails, and trains, and (iii) the fraction of beads in loops, tails, and trains. Here, train refers to a contiguous sequence of beads at the macroion surface, and in this analysis we have used the same definition of $R_c$ as above.

In many theories, a central quantity is the ratio of charges carried by the polyion beads in the collapsed layer and the macroion charge denoted by $|Z_p^c/Z_m|$. This quantity is often taken as a measure of the strength of the polyion−macroion complex. The case of $|Z_p^c/Z_m| < 1$ is referred to as an undercharged complex and $|Z_p^c/Z_m| > 1$ to an overcharged complex. The upper limit of $|Z_p^c/Z_m|$ is $|Z_p/Z_m|$ corresponding to the case were all polyion beads are located in the collapsed layer. Also here $R_c$ has been used as a criterion for collapsed beads. Note the precise value of $|Z_p^c/Z_m|$ depends on $R_c$, so the change, rather than the absolute value, of $|Z_p^c/Z_m|$ should be the focus.

## 3. Results

The structure of the polyion−macroion complexes with different chain stiffnesses will be presented separately. For each stiffness, the structure of the 16 different systems will be explored in the following order: (A) the system with the shortest polyion having the smallest linear charge density ($N_b$, $Z_b$) = (40, 0.25); (B) an increase of the linear charge density with $N_b = 40$; (C) an increase of the chain length with $Z_b = 0.25$; and (D, E, ...) the remaining systems, typically, in the direction of increasing $Z_p = N_b Z_b$, since the change of the structure is less when both $N_b$ and $Z_b$ are varied keeping $Z_p$ fixed.

**3.1. Flexible Polyions.** Figure 1 displays a set of shapshots illustrating the structure of the polyion−macroion complexes involving flexible polyions, and Figure 2 provides the corresponding bead complexation probabilities. In both figures, bead charge, $Z_b$, is increasing along the horizontal axis and the number of beads, $N_b$, along the vertical axis. The letters A−F are included for easier reference. Table 2 provides the complex charge ratios $|Z_p^c/Z_m|$.

(A) Starting with the case of a short polyion ($N_b = 40$) with a small linear charge density ($Z_b = 0.25$), all the polyion beads are located near the macroion surface (Figure 1). The chain is locally folded in a disordered manner, and on average five small loops are formed. Moreover, the polyion is only able to cover a small part of the macroion surface. The complexation probability shows an extended plateau at $P_c \approx 0.6$ consistent with the formation of loops (Figure 2). Such a plateau with high complexation probability will be referred to as a binding region. Only a slightly reduced probability of complexation toward the ends of the chain is found. Thus, a fairly thick, but incomplete, layer of polyion beads is obtained for this system.

(B) As the polyion linear charge density is increased ($Z_b = 0.25 \rightarrow 1$) and still considering a short polyion ($N_b = 40$), there is a gradual transformation to a thinner polyion layer (Figure 1). The average number of loops decreases from 5 to 1.7. The value of the complexation probability in the binding region increases gradually and reaches nearly 1 at $Z_b = 1$. Moreover, the complex charge ratio increases from 0.14 to 0.93 (Table 2), the latter being close to its maximal value 1. Hence, the complex between the short and highly charged polyion ($N_b$, $Z_b$) = (40, 1) and the macroion has a thin, but still incomplete, layer of polyions around the macroion.

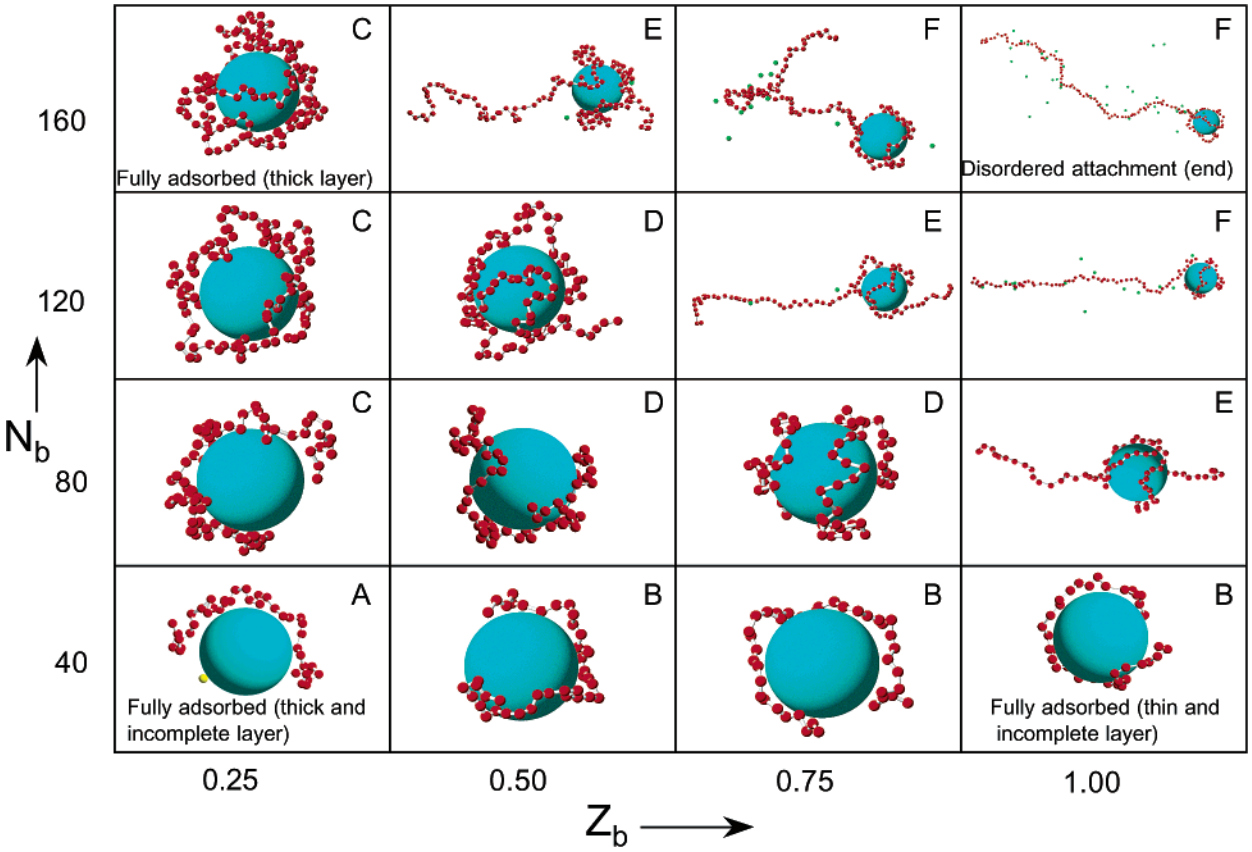


**Figure 1.** Snapshots of the polyion−macroion complex from simulations with the bare persistence length $l_P = 7$ Å. The bead charge is increasing from $Z_b = 0.25$ to $Z_b = 1$ (left to right) and the number of beads is increasing from $N_b = 40$ to $N_b = 160$ (bottom to top). The length scale differs among the shapshots.

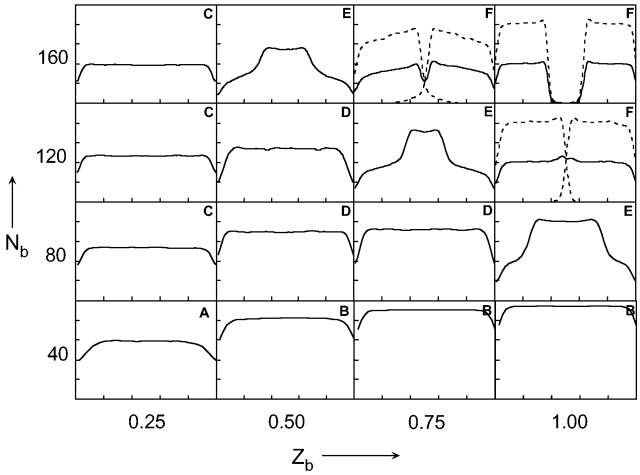


**Figure 2.** Bead complexation probability $P_c(i_b/N_b)$ as a function of the normalized bead number $(i_b/N_b)$ with the bare persistence length $l_P = 7$ Å. The bead charge is increasing from $Z_b = 0.25$ to $Z_b = 1$ (left to right) and the number of beads is increasing from $N_b = 40$ to $N_b = 160$ (bottom to top). In all panels, both the abscissa and the ordinate ranges from 0 to 1. For systems $(N_b, Z_b) = (120, 1)$, (160, 0.75), and (160, 1), $P_c$ for the two asymmetric states (dashed curves) are shown (see text for further details).

(C) Consider now the weakly charged chain ($Z_b = 0.25$). As the chain length is increased ($N_b = 80 \rightarrow 160$), a gradual transformation to a thicker polyion layer is observed and the layer eventually covers the whole macroion surface (Figure 1). The polyion remains locally highly folded, and the number of loops is increasing from 5 to 19. The binding region is still very extended, showing only small end effects (Figure 2). The value of the complexation function in the binding region drops from 0.6 to 0.4. The complex charge ratio increases from 0.14 to 0.38 (Table 2), the latter being much smaller than the maximal value 1. Thus, the complex between the long and weakly charged polyion $(N_b, Z_b) = (160, 0.25)$ and the macroion displays a thick and complete layer of polyion beads.

**TABLE 2: Complex Charge Ratio $|Z_p^c/Z_m|$, Where $Z_p^c$ Denotes the Charge of Collapsed Beads and $Z_m$ the Charge of the Macroion for $l_P = 7$ Å**

| | $Z_b$ | | | |
|---|---|---|---|---|
| $N_b$ | 0.25 | 0.5 | 0.75 | 1 |
| 160 | 0.38 | 0.73 | 0.98 | 1.20 |
| 120 | 0.34 | 0.75 | 0.99 | 1.19 |
| 80 | 0.26 | 0.68 | 1.04 | 1.20 |
| 40 | 0.14 | 0.40 | 0.66 | 0.93 |

(D) Three of the remaining systems $(N_b, Z_b) = (80, 0.5)$, (80, 0.75), and (120, 0.5) display complex structures similar to the previous systems considered. Again, all beads, expect a few ones in short tails, are equally adsorbed and localized in a layer near the macroion (Figures 1 and 2). The two trends, (i) beads being more strongly attracted by the macroion as $Z_b$ is increased at fixed $N_b$ and (ii) an appearance of a thicker adsorbed layer as $N_b$ is increased at fixed $Z_b$, are continued.

(E) Next, consider the systems $(N_b, Z_b) = (80, 1)$, (120, 0.75), and (160, 0.5) with the stoichiometric charge ratio $|Z_p/Z_m| \approx 2$ (diagonally positioned in Figures 1 and 2). A different complex structure appears now; the snapshots show that two polyion tails are now present (Figure 1). The complexation probability functions display the following features: (i) an enhanced binding probability for ca. 40 central beads, (ii) regions with lower probability on each side, and (iii) an even lower probability for ca. 10 beads at the chain ends (Figure 2). As will be further

elaborated below, the system displays an asymmetric binding of the macroion to the polyion (a preference for the polyion to bind toward one side instead of to the center of the polyion), *but* the fluctuations of the tail ends are considerable. Thus, at the condition $|Z_p/Z_m| \approx 2$, a firm complex displays typically two polyion tails of different length, but with considerable tail length fluctuations.

(F) For the three remaining systems ($N_b$, $Z_b$) = (120, 1), (160, 0.75), and (160, 1) with $|Z_p/Z_m| \geq 3$ (top right in Figures 1 and 2), yet other structures are formed. The snapshots show complexes with the macroion bound to one end of the polyions (Figure 1). For symmetry reasons, there is an equal probability of having the polyion bound to either end. In these cases involving an asymmetric binding with two *distinct* end-bounded states, the complexation probabilities averaged over the two states (solid curves) as well as for each of the states separately (dashed curves) are displayed in Figure 2. In systems ($N_b$, $Z_b$) = (120, 1) and (160, 0.75), sufficient transitions between the two states appeared in a single simulation, making $P_c$ symmetric, whereas $P_c$ for the states individually was asymmetric. In system ($N_b$, $Z_b$) = (160, 1), no transition between the two asymmetric states appeared during the production run and $P_c$ was symmetrized after the simulation. The two systems with $Z_b = 1$ have a complex charge ratio ≈1.2, demonstrating *overcharged* macroions. Thus, for flexible chains with the longest and highest linear charge densities considered, the macroion is end-attached to the polyion and overcharged and the beads attached display a disordered structure.

For the flexible polyion, we have hence observed polyion−macroion complexes displaying transitions from no, to two, and finally one tail as the length and/or the linear charge density of the polyion is increased. These transitions have been examined in further detail by considering the tail joint probability function $P(t_1,t_2)$ denoting the probability of having tails of length $t_1$ and $t_2$ simultaneously. The joint probability function is normalized according to $\sum_{t1}\sum_{t2} P(t_1,t_2) = 1$ and has the symmetry property $P(t_1,t_2) = P(t_2,t_1)$. Figure 3 shows $P(t_1,t_2)$ represented as contour diagrams for systems with $Z_b = 1$ and $N_b = 40$, 80, and 120. The configurations specified by $(t_1,t_2)$ with the largest probability are marked with solid circles, and their values will be referred to as $P_{max}$. The equiprobability contour curves are separated by factors of 2. We also notice that the simulated joint probability functions nearly obey the symmetry requirement.

With the smallest chain length, Figure 3a displays that the largest probability appears at $(t_1,t_2) = (0,0)$. The probability decreases rapidly and continuously for configurations with successively more beads in the tails, the distribution of the beads between the two tails being of no importance. The small probability of having tails even composed of just a few beads is consistent with the very extended binding region given in Figure 2. With the next chain length, Figure 3b displays a diagonal band of significant probability extending from $t_{tot} \equiv t_1 + t_2 \approx 15-25$ with high probability at $t_{tot} \approx 20$. The largest probability appears at $(t_1,t_2) = (0, 20)$ and (20, 0), whereas the probability at the saddle point is $P(12,12) \approx P_{max}/15$. Thus, there is a considerable fluctuation of the total number of beads being in tails and a large fluctuation of the length of a single tail. Since the largest probability of a given configuration appears off the $t_1 = t_2$ diagonal, the system is classified as being an asymmetric one. Despite the fact that $P_{max}$ appears for a one-tail configuration, the extensive fluctuations involving two-tail configurations imply that the complex should be characterized as a two-tail state (with tails of different lengths). Figure 3c displays the corresponding contour diagram for $N_b = 120$. The

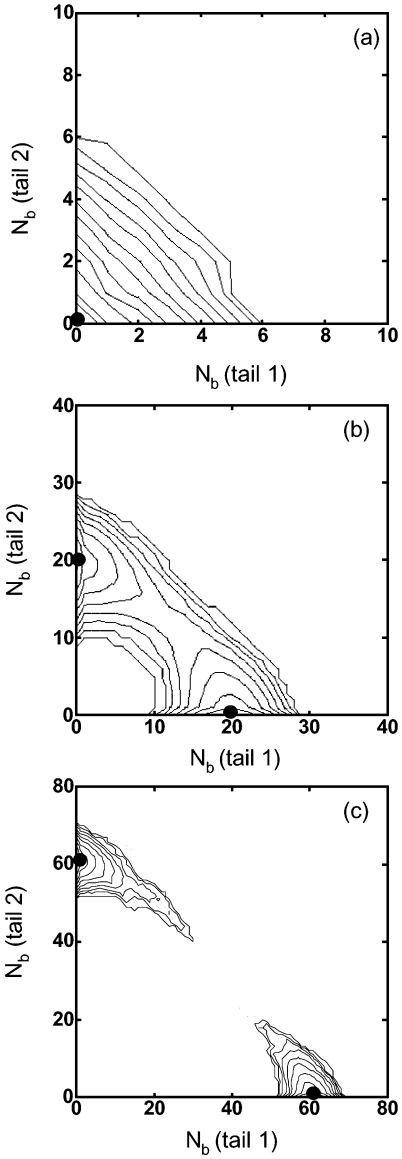


**Figure 3.** Tail joint probability function $P(t_1, t_2)$ denoting the probability that a complex possesses two tails composed of $t_1$ and $t_2$ beads, respectively, for systems ($N_b$, $Z_b$) = (a) (40, 1), (b) (80, 1), and (c) (120, 1). The maximum probabilities are 0.56, 0.026, and 0.057, respectively, and solid spheres indicate their positions. The equiprobability contour curves start at 0.5, 0.025, and 0.05, respectively, and the probability of consecutive curves differs by a factor of 2.

largest probability appears at $(t_1,t_2) \approx (0, 61)$ and (61, 0); hence an asymmetric binding is again found. The probability decreases rapidly at small deviations from the optimal conditions; thus fluctuations are small, and this complex is well-described as a one-tail state. The corresponding contour diagram for $N_b = 160$ (not shown) continues the trend found in Figure 3. Very pronounced probability maxima appear at $(t_1,t_2) \approx (0, 100)$ and (100, 0). Moreover, the contour diagrams for ($N_b$, $Z_b$) = (160, 0.5) and (120, 0.75) resemble that for (80, 1), displaying pronounced probability maxima on the axes with a diagonal band of extended probability connecting these two regions demonstrating substantial tail length fluctuations.

At this stage, the shape of the complexation probability functions for systems ($N_b$, $Z_b$) = (80, 1), (120, 0.75), and (160, 0.5) can be better understood. In system ($N_b$, $Z_b$) = (160, 1), 60 beads are directly involved in the complexation with the macroion. With $N_b = 160$ and an end-binding arrangement, a clear separation of the two binding regions for

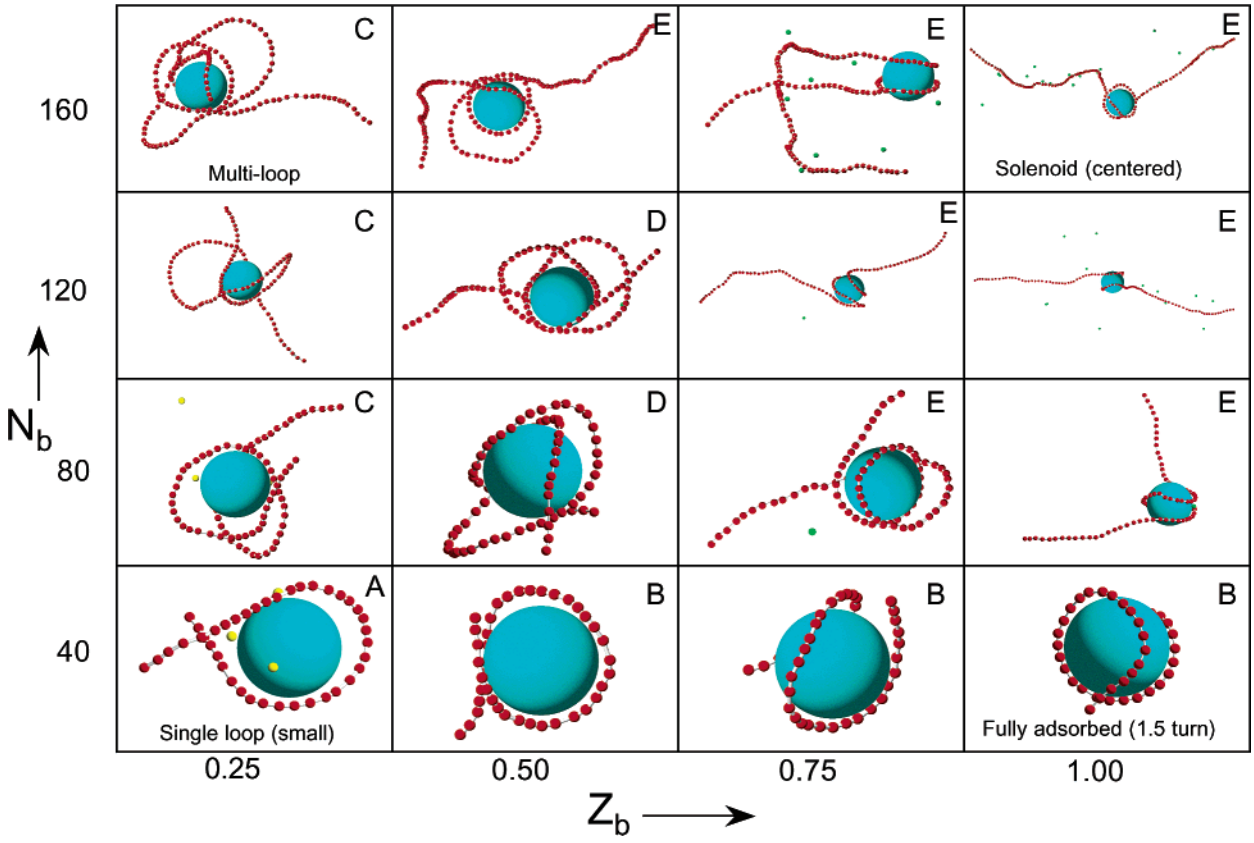


**Figure 4.** Same as Figure 1, but $l_P = 250$ Å.

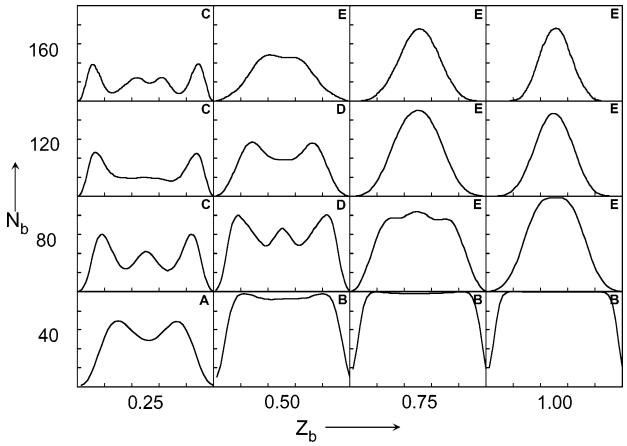


**Figure 5.** Same as Figure 2, but $l_P = 250$ Å.

the two one-tail states appears in the average complexation probability function (see Figure 2, top-right panel, solid curve). However, as the chain length decreases, these two binding regions become closer. With $N_b = 120$ (=2 × 60), they just touch each other (see Figure 2, second-top-right panel), whereas with $N_b = 80$ they overlap each other, giving rise to the peculiar shape of the complexation probability function (see Figure 2, second-bottom-right panel). The same type of overlap appears for systems ($N_b$, $Z_b$) = (120, 0.75) and (160, 0.5).

**3.2. Semiflexible Polyions.** The case of semiflexible chains with bare persistence length $l_P = 250$ Å will now be considered. The shapshots illustrating the structure of the polyion−macroion complexes are provided in Figure 4, whereas the corresponding bead complexation probabilities are given in Figure 5 and the complex charge ratios in Table 3.

(A) With the short and weakly charged polyion chain ($N_b$, $Z_b$) = (40, 0.25), one short loop and two short tails appear (Figure 4). The minimum in the central region displayed by the complexation binding is shallow (Figure 5), and the loop analysis showed that an average loop length involves eight beads. As compared to the corresponding flexible chain, the tails are here more pronounced and the complex charge ratio somewhat smaller.

**TABLE 3: Complex Charge Ratio $|Z_p^c/Z_m|$, Where $Z_p^c$ Denotes the Charge of Collapsed Beads and $Z_m$ the Charge of the Macroion for $l_P = 250$ Å**

| | $Z_b$ | | | |
|---|---|---|---|---|
| $N_b$ | 0.25 | 0.5 | 0.75 | 1 |
| 160 | 0.20 | 0.52 | 0.82 | 0.88 |
| 120 | 0.18 | 0.52 | 0.84 | 0.89 |
| 80 | 0.17 | 0.54 | 0.81 | 0.94 |
| 40 | 0.11 | 0.41 | 0.67 | 0.90 |

(B) As the polyion linear charge density is increased ($Z_b$ = 0.25→1), the beads become more firmly attached to the macroion (Figure 4). The complexation probability function shows that the central loop is gradually vanishing and that the binding probability in the binding region is continueously increasing and approaches ≈1 for $Z_b = 1$ (Figure 5). Thus, for the highest charged polyion, the polyion is fully adsorbed and makes a 1.5 turn around the macroion.

(C) As the polyion length is increased ($N_b$ = 80→160), again starting from the system ($N_b$, $Z_b$) = (40, 0.25), a gradual appearance of more loops occurs (Figure 4). At $N_b = 80$, two loops with an average length of 16 beads are present. For the two longer polyions no distinct pattern appears, except that two sections centered ≈20 beads from each ends display enhanced binding probability (Figure 5). However, the loop analysis shows that on the average 2.6 and 3.0 loops are formed involving 24 and 32 beads, respectively. These systems are hence characterized by considerable fluctuations in the number and length of

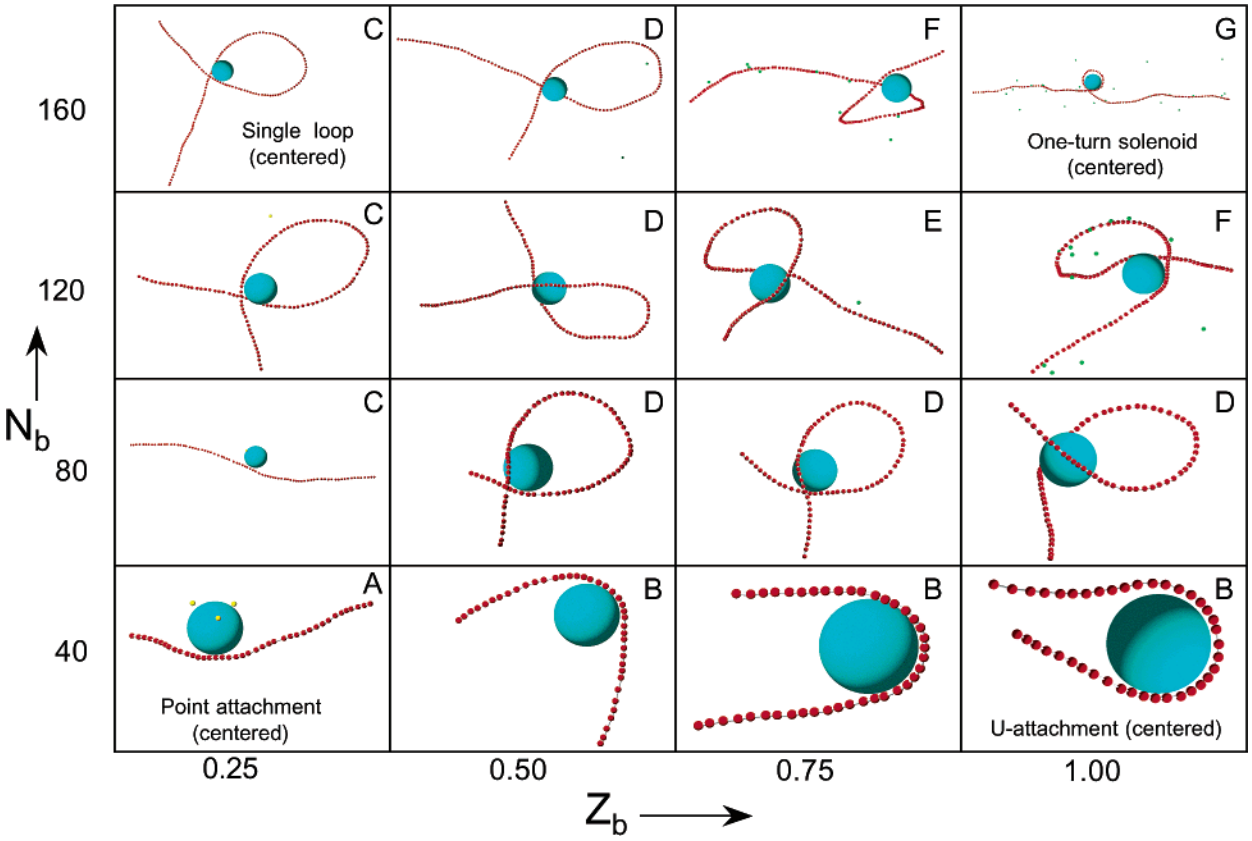


**Figure 6.** Same as Figure 1, but $l_P = 1000$ Å.

loops and their location along the central part of the chain contour. The complex charge ratio stays low as $N_b$ is increased (Table 3). Thus, with a long and weakly charged chain, the complex displays a highly fluctuating multiloop arrangement.

(D) The two systems ($N_b$, $Z_b$) = (80, 0.5) and (120, 0.5) display the same trend as the corresponding systems but with $Z_b = 0.25$ (Figures 4 and 5). The beads are however closer to the macroion (larger $P_c$) due to the stronger electrostatic bead−macroion attraction, and on the average ≈2 loops are formed. With $N_b = 120$ more extended tails start to develop (Figures 4 and 5).

(E) As the chain length and/or the linear charge density is increased further, the remaining seven systems possess similar structure. The polyion is wound ≈1.5 turns around the polyion and has on average two symmetric tails (symmetric binding). The short solenoid is looser at $Z_b = 0.5$ and tighter at $Z_b = 1$ (Figure 5). For system ($N_b$, $Z_b$) = (160, 1) special efforts were made to exclude the possibility of a one-tail state. In more detail, the final end-binding configuration obtained with $l_P = 7$ Å was taken as a start configuration. The macroion was temporarily *fixed* at the end of the chain, while the chain was relaxed at the new persistence length $l_P = 250$ Å. As the constraint was released and the equilibration proceeded, the centered-solenoid structure was re-formed, demonstrating a preference for the two-tail state. Table 3 shows $|Z_p^c/Z_m| < 1$ for all systems; hence we have *undercharged* macrioions.

Thus, as the chain stiffness is increased from $l_P = 7$ to 250 Å, a considerable change in the structure of the polyion−macroion complex appears. At small $N_b$ or small $Z_b$, the structure of the attached beads is disordered at $l_P = 7$ Å, whereas a short solenoid (small $N_b$ and large $Z_b$) or a multiloop structure (large $N_b$ and small $Z_b$) is present at $l_P = 250$ Å. When both $N_b$ and $Z_b$ are large, tails are developed independent of the persistence length, but at $l_P = 7$ Å an overcharged one-tail state appears as compared to an undercharged two-tail state at $l_P = 250$ Å. The transition from the one-tail to two-tail state at ($N_b$, $Z_b$) = (160,1) as $l_P$ is increased from $l_P = 7$ to 150 Å was investigated in more detail for intermediate $l_P$. In particular, at $l_P = 60$ Å the one-tail and two-tail states appeared with roughly equal probability and frequent transitions between them appeared. To conclude, a flexible polyion gives rise to an end-bound macroion with one tail (asymmetric binding), and as $l_P$ is increased, there is a gradual transition to a center-solenoid complex with two tails (symmetric binding). We also notice that the complex charge ratio $|Z_p^c/Z_m|$ decreases from 1.2 to 0.88 in this process.

**3.3. Stiff Polyions.** The stiff chains considered possess the bare persistence length $l_P = 1000$ Å. The shapshots illustrating the structure of the polyion−macroion complexes are provided in Figure 6, while the corresponding bead complexation probabilities are given in Figure 7 and the complex charge ratios are collected in Table 4.

(A) With the short and weakly charged polyion chain, only a few beads are in close contact with the macroion surface and the polyion is stretched (Figure 6) and the bead complexation probability displays a maximum for central beads (Figure 7). The complex charge ratio is very small, 0.04 (Table 4). This symmetric binding is referred to as a centered point attachment.

(B) As the polyion linear charge density is increased, the stretched chain is continuously changed to a U-turn conformation (Figure 6). The complexation probability for central beads increases, showing a stronger attachment for these beads, and the binding region becomes more extended (Figure 7). At the highest linear charge density, ca. 20 beads are closely attached to the macroion and on average two symmetric tails are present. The complex charge ratio increases to 0.50 (Table 4). Thus, at $Z_b = 1.0$, a centered U-attached structure has been developed.

(C) As the polyion length is increased, the centered point attachment first remains ($N_b = 80$), while at longer chain lengths

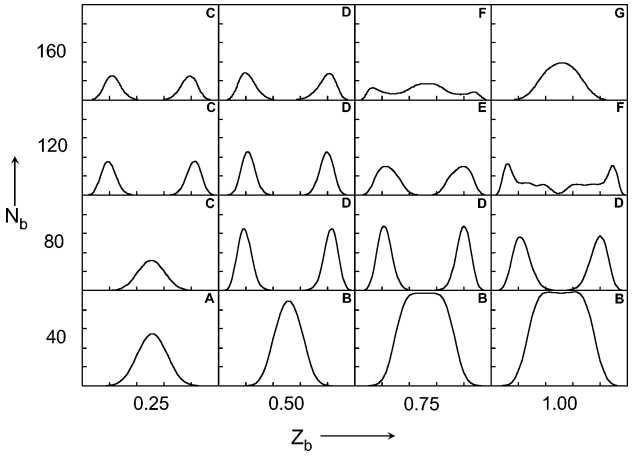


**Figure 7.** Same as Figure 2, but $l_P = 1000$ Å.

**TABLE 4: Complex Charge Ratio $|Z_p^c/Z_m|$, Where $Z_p^c$ Denotes the Charge of Collapsed Beads and $Z_m$ the Charge of the Macroion for $l_P = 1000$ Å**

| | $Z_b$ | | | |
|---|---|---|---|---|
| $N_b$ | 0.25 | 0.5 | 0.75 | 1 |
| 160 | 0.074 | 0.17 | 0.27 | 0.64 |
| 120 | 0.072 | 0.17 | 0.27 | 0.36 |
| 80 | 0.039 | 0.17 | 0.27 | 0.36 |
| 40 | 0.037 | 0.11 | 0.33 | 0.50 |

($N_b = 120$ and 160) a transition to a centered single-loop configuration appears (Figures 6 and 7). The two peaks in the complexation probability function become broader and possess lower amplitude for the longer chain, implying larger fluctuations of the location of the macroion along the chain contour. The complex charge ratio remains small (Table 4). Thus, with a long and weakly charged chain, the complex displays a centered single-loop arrangement.

(D) Five of the remaining nine systems, all except those four located in the top-right corner in the ($N_b$, $Z_b$) square, display a single loop with limited local fluctuations (Figures 6 and 7) similar to those in systems ($N_b$, $Z_b$) = (120, 0.25) and (160, 0.25). The translational fluctuations along the chain contour increase as the chain length is increased at $Z_b = 0.50$, as well as the linear charge density is increased at $N_b = 80$.

(E) The complex at ($N_b$, $Z_b$) = (120, 0.75) also possesses a single loop, but the loop is now twisted. The stronger attraction between the loop beads and the macroion partly folds the loop toward the macroion. The complexation probability function displays two broad peaks, implying substantial translational fluctuations along the chain contour.

(F) For two of the remaining systems ($N_b$, $Z_b$) = (160, 0.75) and (120, 1) with $|Z_p/Z_m| = 3$, still a single loop appears (Figure 6 and the loop analysis), but the complexation probability function has now lost its previous simplicity (Figure 7). To facilitate the analysis, Figure 8 displays the tail joint probability functions for these systems. Starting with ($N_b$, $Z_b$) = (160, 0.75), the loop, tail, and train analysis determines that on average 71 beads are involved in one loop and 7 beads in each of the two attachment points. Figure 8a shows that the state with tail lengths $\approx$60 and $\approx$18 has the largest probability. Hence, we have an asymmetric binding with two unequal sized tails with one attachment point located near the center of the chain and the other ca. 20 beads from one end. The complexation probability function shown is an average of a function having two peaks located at $i_b \approx 20$ and 85, respectively, and its mirror image.

Considering the other system ($N_b$, $Z_b$) = (120, 1), the average loop length is 61 beads and again 7 beads are involved in each attachment point. The corresponding joint probability function, however, reveals a more complex situation. Although the maximal probability appears for unequal tail lengths as for the previous system, there are large fluctuations in the length of the longer tail with the length of the shorter one less affected (see dashed curves in Figure 8b). Assuming that the number of the beads in the attachment points is constant, this implies a considerable variation of the loop length. This fluctuation in loop length is viewed as a competition between (i) a strong electrostatic attraction between the beads in the loop and the macroion (favor a short loop) and (ii) the bending energy preventing the loop to have a high curvature (favor a large loop). With a stronger bead−macroion attraction or a weaker bending energy, the transition to a short solenoid (see corresponding shapshot in Figure 4) would be completed. The situation is even more complicated; a small free energy barrier for the longer tail to attain two different lengths implying a corresponding barrier between loops of two different lengths is present (Figure 8b). Such an appearance of two different loop lengths also appeared for the system ($N_b$, $Z_b$) = (120, 0.75) (data not shown). Further studies are required to evaluate their significance.

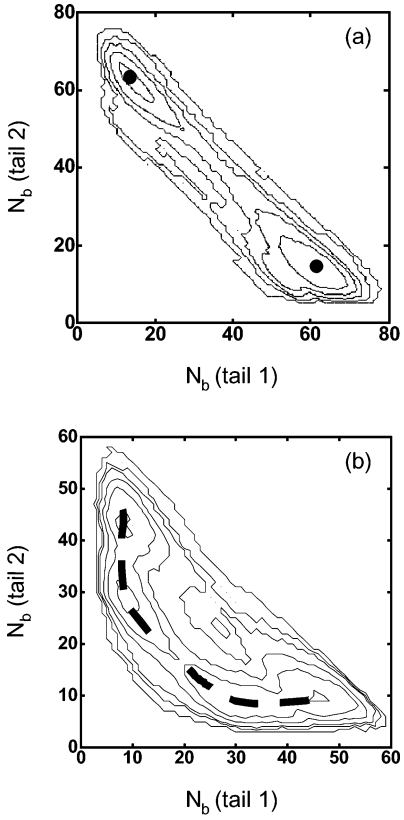


**Figure 8.** Joint probability function $P(t_1, t_2)$ denoting the probability that a complex possesses two tails composed of $t_1$ and $t_2$ beads, respectively, for systems ($N_b$, $Z_b$) = (a) (160, 0.75) and (b) (120, 1). The maximum probabilities are 0.0025 and 0.0021, respectively. In (a) solid spheres indicate the positions of maximal probabilities, and in (b) dashed curves indicate extended regions with high probability. The equiprobability contour curves start at 0.0021 and 0.0019, respectively, and the probability of consecutive curves differs by a factor of 2.

(G) Depending on the starting configuration, the system ($N_b$, $Z_b$) = (160, 1) displayed two different structures: a center-solenoid and an end-loop state. The potential energy difference between the two states is $\approx 20kT$. The free energy barrier between the two states is too large to observe transitions between the two states. The properties of the end-loop state are similar

**TABLE 5: Specification of Systems Simulated by Different Groups[a]**

| | Mateescu et al.[b] | Nguyen and Shklovskii[c] | Chodanowski and Stoll[d] | Akinchina and Linse |
|---|---|---|---|---|
| $R_b$ (Å) | 0.71 | 1.42 | 3.57 | 2.0 |
| $N_b$ | 100 | 130−180 | 25−200 | 40, 80, 120, 160 |
| $Z_b$ | 1 | 1 | 1 | 0.25, 0.5, 0.75, 1 |
| $R_{bb}$ (Å) | 1.4 | 7.14 | 7.14 | 5.5 |
| $R_m$ (Å) | 9.2−10.7 | 28.4 | 35.7 | 20 |
| $Z_m$ | −50 | −100 | −100 | −40 |

[a] Bjerrum length $l_B \approx e^2/(4\pi\epsilon_0\epsilon_r kT) \approx 7.14$ Å throughout. [b] Reference 17. Length properties converted from reduced units to angstroms using $Z_b = 1$ and $l_B = 7.14$ Å. [c] Reference 21. [d] Reference 32.

to those of the system $(N_b, Z_b) = (160, 0.75)$. The center solenoid contains only one tight turn (Figure 6, top-right corner), involving ≈25 beads, and the complexation distribution function displays large fluctuations of the position of the macroion along the polyion contour (Figure 7). The length of the tails varies between 35 and 100 beads. The degree of undercharging continues to decrease as compared to the less stiff chains (cf. Tables 2−4).

## 4. Discussions

Some results from recent theoretical and simulation studies on the polyion−macroion complexation will be discussed and compared with our data.

**4.1. Flexible Polyions.** Regarding flexible polyions, Mateescu et al.[17] and Nguyen and Shklovsii[21] have presented relevant theoretical predictions complemented with simulations and Chodanowski and Stoll[32] have performed a more extensive simulation study. Both theories are based on free energy expressions containing different contributions and subjected to a minimization with respect to the length of the tail(s). All simulations employ models containing a flexible polyion composed of a sequence of charged hard spheres interacting with a single, oppositely charged hard sphere representing a macroion. The details of the bead−bead bond potential differ, but it is believed to be of minor importance. For convenience, the values of the important parameters are given in Table 5, using a common notation. In the following, we will examine the transition collapsed polyion → appearance of tail(s) as $N_b$ is increased for salt-free systems.

The predictions of the theory by Mateescu et al.[17] was discussed using $R_m$ as an independent variable. Briefly, as $R_m$ is increased at $Z_m = 50$, the theory predicts (i) a continuous "two-tail state" → "collapsed state" transition for $1 < |Z_p/Z_m| \leq 1.6$, (ii) a first-order "two-tail state" → "collapsed state" transition for $1.6 < |Z_p/Z_m| \leq 2.0$, and (iii) first-order "two-tail state" → "one-tail state" → "collapsed state" transitions for $|Z_p/Z_m| > 2.0$ (see Figure 1 of ref 17). This implies that as $N_b$ is increased, the theory predicts (i) a "collapsed state" → "two-tail state" transition for small $R_m$ and (ii) "collapsed state" → "one-tail state" → "two-tail state" transitions for larger $R_m$. (This was confirmed by additional calculations by us.) Applying their theory to our conditions with $Z_b = 1$, we find a "collapsed state" → "two-tail state" transition as $N_b$ is increased. Moreover, in their simulations at $|Z_p/Z_m| = 2$, they observed a discrete reduction from ≈96 to ≈85 collapsed beads at the "collapsed state" → "two-tail state" transition as $R_m$ was decreased. From their snapshots they concluded that, close to the collapsed state, "the system oscillates between the two-tail and one-tail configurations".

The theory by Nguyen and Shklovskii[21] predicts first-order "overcharged collapsed state" → "overcharged one-tail state" → "undercharged two-tail state" transitions as $N_b$ is increased. At the conditions given in Table 5, the first transition appeared at $|Z_p/Z_m| \approx 1.4$, where the number of collapsed beads decreased by ≈10%. This transition was verified by simulation, but no discussions of any tail fluctuations were made. The second transition was predicted to appear first for very long polyions. Applying their theory to our case with $Z_b = 1$, we found that $N_b \approx 9700$ is required.

In their study, Chodanowski and Stoll[32] found a "collapsed overcharged state" → "overcharged one-tail state" transition at $N_b = 151$ accompanied by a reduction of the number of collapsed beads, in perfect agreement with the theory by Nguyen and Shklovskii. Moreover, the authors say that "...complexes with two tails were not observed during our simulations", as found in our study.

All relevant results in refs 17, 21, and 32 and from our simulation *support, or are at least consistent with,* the following sequence of states as $N_b$ is increased:

(i) collapsed state →

(ii) fluctuating two-tail state →

(iii) overcharged one-tail state →

(iv) undercharged two-tail state.

We notice that the fluctuating two-tail state is only described in some of the simulations (Mateescu et al. and ours) and that the two theories were not constructed to describe this state. Moreover, only the theories predict the final undercharged two-tail state; long polyions are required making simulation less suited for describing this state. Finally, the theory by Mateescu et al. requires a certain macroion size to predict an overcharged one-tail state.

The driving force for the sequence of transitions is the more rapidly increasing bead−bead repulsion as compared to the bead−macroion attraction as $N_b$ is increased. The "overcharged collapsed state" → "overcharged one-tail state" transition is a typical example, where the increasing bead−bead repulsion eventually forces some of the beads to be removed from the collapsed layer. At the "overcharged one-tail state" → "undercharged two-tail state" transition, favorable bead−macroion attraction is now sacrificed (i) to diminish the repulsion among the collapsed beads by reducing the number of them, (ii) to reduce the repulsion among the tail beads by increasing their separation, and (iii) making the tail-complex interaction attractive.

**4.2. Variation of Polyion Flexiblity.** Schiessel et al.[22] have proposed a theory describing the structure of complexes formed by one semiflexible chain interacting with a point via short-range attraction. This theory was recently extended by Schiessel[24] to cover the case with an electrostatic interaction between the chain and a central macroion at different ionic strength. The theory is also based on an expression of the free energy of the system. A brief comparison with the latter study at low ionic strength will be made here.

The relevant results were summarized by Schiessel as a state diagram describing the structure of the complexes as a function of the polyion length $L$ and a parameter with dimension length describing the ratio of the persistence length and the strength of the bead−macroion interaction, here denoted by $X$ (see Figure 2 of ref 24). The main features are as follows:

(i) At small $X$ (e.g. corresponding to flexible polyions), a transition from a collapsed state to a one-tail state was envisioned as $L$ is increased.

(ii) As $X$ is increased, a continuous transition from a collapsed state to a state possessing loops (referred to as leaves in ref 24) appears at $X = X^*$ and $X^*$ is independent of $L$.

(iii) As $L$ is increased, the number of loops appearing at $X^*$ becomes larger, and for a sufficiently small $L$ no loops appear.

(iv) Finally, as $X$ ($>X^*$) is increased (e.g. corresponding to stiffer chain), the number of loops is decreasing.

Prediction (i) was just discussed, and it agrees with previous studies; apart from that, the question of one or two tails was not addressed by Schiessel. Prediction (ii) was supported in paper 1 at the condition $|Z_p/Z_m| = 1$, where we observed a transition from a collapsed state to a multiloop state as the chain stiffness was increased. The strongest support for prediction (iii) appeared in Figure 4. At $Z_b = 0.25$ and 0.5, we observed an increased number of loops as $N_b$ was increased. The case with larger electrostatic coupling ($Z_b = 0.75$ and 1), at which no prominent loops appeared, would correspond to $X < X^*$ in Figure 2 of ref 24. Prediction (iv) was also observed in paper 1, where at $|Z_p/Z_m| = 1$ a successive transition from a multiloop state to a single-loop appeared as the chain stiffness was increased. The same qualitative trend appeared also at $|Z_p/Z_m| = 1/2$, where, e.g., snapshots for system ($N_b$, $Z_b$) = (80, 0.25) in Figure 4 at $l_P = 250$ Å displayed two loops and in Figure 6 at $l_P = 1000$ Å no loops. Similarly, at $|Z_p/Z_m| = 1.5$ the system ($N_b$, $Z_b$) = (120, 0.5) displayed a reduction from two to one loop as $l_P$ was increased from 250 to 1000 Å. Thus, it appears that our results qualitatively support the picture provided by the theory by Schiessel. However, further tailored simulations have to be performed to assess all predictions, in particular that $X^*$ is independent of $L$.

**4.3. Stiff Polyions.** An extensive theoretical examination of the collapse−uncollapse transition has been made by Kunze and Netz.[20] They selected the model system to represent DNA complexing a histone. The theory is based on a free energy functional to be minimized with respect to the polyion conformation. Their principal variables were the charge of the histone and the screening length. The relatively small overlap in parameter variation limits the possibility of making a more detailed comparison. Nevertheless, from our simulations we infer that large loops suppressed in their theory are important.

## 5. Summary

The complexation between one polyion and one spherical macroion in the limit of weak electrostatic screening has been examined on the basis of Monte Carlo simulations. We have examined the structure of the complex at three different persistence lengths. For each chain stiffness, a systematic variation of the chain length and linear charge density of the chain was undertaken. The polyion charge to macroion charge ratio was varied from 1/4 to 4. This study is an extension of our previous one,[37] where systems restricted to the charge ratio equal to one were considered.

The system possesses a large number of reduced parameters.[37] Despite the fact that we have only varied three of them, a very rich structural behavior was found. This variation of structure arises from an intricate interplay between (i) the attractive bead−macroion interaction which favors complexation, (ii) the repulsive bead−bead interaction which opposes complexation, (iii) the bending energy which also restricts the ability of the chain to complex the macroion, (iv) the repulsive/attractive tail−complex interaction, and (v) the large number of degrees of freedom associated with the polyion chain.

With a flexible chain, we observed a successive transition from a fully adsorbed chain forming a rather thick but incomplete collapsed layer to a corresponding thin layer as the bead charge was increased for a short polyion. The thick but incomplete collapsed layer became even thicker and covered the full macroion surface as the polyion length was increased. In the case of a long and highly charged polyion, the macroion became end-attached (asymmetric binding) to the polyion with the adsorbing beads being in a disordered manner. Moreover, we have examined in detail the transition from a collapsed state to the end-attached state and found a broad intermediate regime with large fluctuations in tail lengths, where the system preferentially should be considered as having two tails. In this aspect, previous simulations have not yet provided a clear picture.

With a semiflexible chain, a small single loop appeared for the short and weakly charged polyion and the loop gradually vanished as the bead charge was increased. However, as the chain length was increased, the number of loops increased and for the longest polyion the complex was characterized as a multiloop state. In the limit of a long and highly charged polyion, an undercharged complex with the chain forming a solenoid with two symmetric tails was observed (symmetric binding).

Finally, with a stiff chain, the number of loops was reduced. For the shortest polyion, no loops appeared; here a point attachment was converted to a U-attachment as the linear charge density was increased. Otherwise, in most cases only one loop appeared, the loop being twisted by the large electrostatic attraction between beads and the macroion at sufficiently long polyion and high linear charge density. In the limit of a long and highly charged polyion, the central solenoid (symmetric binding) will probably become the dominating state.

The prediction of recent theories and results of previous and related simulations have been discussed. For flexible polyions, a coherent picture of the structural changes as the polyion length is increased has been proposed. In this limit, the competing bead−macroion and bead−bead interactions are essential for describing the complex. Moreover, our results display a qualitative agreement with the theory by Schiessel, which focused on the balance between the attractive bead−macroion interaction and the chain bending stiffness. Due to the rich behavior, no theory yet describes all main aspects of the polyion−macroion complexation.

**Acknowledgment.** We thank Helmut Schiessel for discussions and for sending his work[24] prior to publication, Roland Netz for sending their work[20] also prior to publication, and Magnus Ullner for helpful discussions.

## References and Notes

(1) Goddard, E. D. *Colloids Surf.* **1986**, *19*, 255.
(2) *Polymer-Surfactant Systems*; Kwak, J. C. T., Ed.; Dekker: New York, 1998; Vol. 77.
(3) Lindman, B.; Thalberg, K. Polymer-Surfactant Interactions−Recent Developments. In *Interactions of Surfactants with Polymers and Proteins*; Goddard, E. D., Ananthapadmanabhan, K. P., Eds.; CRC Press: Boca Raton, FL, 1993; p 203.
(4) Hansson, P.; Lindman, B. *Curr. Opin. Colloid Interface Sci.* **1996**, *1*, 604.
(5) Doublier, J. L.; Garnier, C.; Renard, D.; Sanchez, C. *Curr. Opin. Colloid Interface Sci.* **2000**, *5*, 202.
(6) Shubin, V.; Samoshina, Y.; Menshikova, A.; Evseeva, T. *Colloid Polym. Sci.* **1997**, *275*, 655.
(7) Shubin, V. *J. Colloid Interface Sci.* **1997**, *191*, 372.
(8) Marques, E. F.; Regev, O.; Khan, A.; Miguel, M. D.; Lindman, B. *Macromolecules* **1999**, *32*, 6626.
(9) Mashl, R. J.; Gronbech-Jensen, N.; Fitzsimmons, M. R.; Lutt, M.; Li, D. Q. *J. Chem. Phys.* **1999**, *110*, 2219.
(10) Wang, Y. L.; Kimura, K.; Dubin, P. L.; Jaeger, W. *Macromolecules* **2000**, *33*, 3324.
(11) Wang, Y. L.; Dubin, P. L.; Zhang, H. W. *Langmuir* **2001**, *17*, 1670.
(12) Zhang, H. W.; Ohbu, K.; Dubin, P. L. *Langmuir* **2000**, *16*, 9082.
(13) Fuchs, A.; Killmann, E. *Colloid Polym. Sci.* **2001**, *279*, 53.
(14) von Goeler, F.; Muthukumar, M. *J. Chem. Phys.* **1994**, *100*, 7796.
(15) Gurovitch, E.; Sens, P. *Phys. Rev. Lett.* **1999**, *82*, 339.

(16) Park, S. Y.; Bruinsma, R. F.; Gelbart, W. M. *Europhys. Lett.* **1999**, *46*, 454.
(17) Mateescu, E. M.; Jeppesen, C.; Pincus, P. *Europhys. Lett.* **1999**, *46*, 493.
(18) Netz, R. R.; Joanny, J. F. *Macromolecules* **1999**, *32*, 9026.
(19) Kunze, K.-K.; Netz, R. R. *Phys. Rev. Lett.* **2000**, *85*, 4389.
(20) Kunze, K.-K.; Netz, R. R. *Phys. Rev. E* **2002**, *66*, 011918.
(21) Nguyen, T. T.; Shklovskii, B. I. *Physica A* **2001**, *293*, 324.
(22) Schiessel, H.; Rudnick, J.; Bruinsma, R. F.; Gelbart, W. M. *Europhys. Lett.* **2000**, *51*, 237.
(23) Schiessel, H.; Bruinsma, R. F.; Gelbart, W. M. *J. Chem. Phys.* **2001**, *115*, 7245.
(24) Schiessel, H. *Macromolecules* **2003**, *36*, 3424.
(25) Nguyen, T. T.; Shklovskii, B. I. *J. Chem. Phys.* **2001**, *114*, 5905.
(26) Nguyen, T. T.; Shklovskii, B. I. *J. Chem. Phys.* **2001**, *115*, 7298.
(27) Wallin, T.; Linse, P. *Langmuir* **1996**, *12*, 305.
(28) Wallin, T.; Linse, P. *J. Phys. Chem.* **1996**, *100*, 17873.
(29) Wallin, T.; Linse, P. *J. Phys. Chem. B* **1997**, *101*, 5506.
(30) Wallin, T.; Linse, P. *J. Chem. Phys.* **1998**, *109*, 5089.
(31) Kong, C. Y.; Muthukumar, M. *J. Chem. Phys.* **1998**, *109*, 1522.
(32) Chodanowski, P.; Stoll, S. *Macromolecules* **2001**, *34*, 2320.
(33) Chodanowski, P.; Stoll, S. *J. Chem. Phys.* **2001**, *115*, 4951.
(34) Jonsson, M.; Linse, P. *J. Chem. Phys.* **2001**, *115*, 3406.
(35) Jonsson, M.; Linse, P.*J. Chem. Phys.* **2001**, *115*, 10957.
(36) Skepö, M.; Linse, P. *Macromolecules* **2003**, *36*, 508.
(37) Akinchina, A.; Linse, P. *Macromolecules* **2002**, *35*, 5183.
(38) *Computer Simulation of Liquids*; Allen, M. P., Tildesley, D. J., Eds.; Oxford University Press: New York, 1987.
(39) *MOLSIM*, Ver. 3.3.7; Linse, P., Lund University, Sweden, 2002.